Acta Biomaterialia 17 (2015) 16–25

Contents lists available at ScienceDirect

Acta Biomaterialia

journal homepage: www.elsevier.com/locate/actabiomat

Hydroxyapatite reinforced collagen scaffolds with improved architecture and mechanical properties ☆

Robert J. Kane, Holly E. Weiss-Bilka, Matthew J. Meagher, Yongxing Liu, Joshua A. Gargac, Glen L. Niebur, Diane R. Wagner, Ryan K. Roeder *

Department of Aerospace and Mechanical Engineering, Bioengineering Graduate Program, University of Notre Dame, Notre Dame, IN 46556, USA

ARTICLE INFO

Article history:
Received 10 November 2014
Received in revised form 9 January 2015
Accepted 15 January 2015
Available online 30 January 2015

Keywords:
Bioactivity
Collagen
Hydroxyapatite
Osteoinduction
Scaffold

ABSTRACT

Hydroxyapatite (HA) reinforced collagen scaffolds have shown promise for synthetic bone graft substitutes and tissue engineering scaffolds. Freeze-dried HA–collagen scaffolds are readily fabricated and have exhibited osteogenicity *in vivo*, but are limited by an inherent scaffold architecture that results in a relatively small pore size and weak mechanical properties. In order to overcome these limitations, HA–collagen scaffolds were prepared by compression molding HA reinforcements and paraffin microspheres within a suspension of concentrated collagen fibrils (~180 mg/mL), cross-linking the collagen matrix, and leaching the paraffin porogen. HA–collagen scaffolds exhibited an architecture with high porosity (85–90%), interconnected pores ~300–400 μm in size, and struts ~3–100 μm in thickness containing 0–80 vol% HA whisker or powder reinforcements. HA reinforcement enabled a compressive modulus of up to ~1 MPa, which was an order of magnitude greater than unreinforced collagen scaffolds. The compressive modulus was also at least one order of magnitude greater than comparable freeze-dried HA–collagen scaffolds and two orders of magnitude greater than absorbable collagen sponges used clinically. Moreover, scaffolds reinforced with up to 60 vol% HA exhibited fully recoverable elastic deformation upon loading to 50% compressive strain for at least 100,000 cycles. Thus, the scaffold mechanical properties were well-suited for surgical handling, fixation, and bearing osteogenic loads during bone regeneration. The scaffold architecture, permeability, and composition were shown to be conducive to the infiltration and differentiation of adipose-derive stromal cells *in vitro*. Acellular scaffolds were demonstrated to induce angiogenesis and osteogenesis after subcutaneous ectopic implantation by recruiting endogenous cell populations, suggesting that the scaffolds were osteoinductive.

1. Introduction

Bone grafts are commonly used to repair bone defects, such as those caused by traumatic injuries or the resection of osteosarcoma, and to promote implant fixation, such as in spinal fusion and dental implants [1–3]. Autograft is the current gold standard used in the majority of procedures but is limited by supply, graft size, and donor-site morbidity [1–5]. Allograft can be used to obviate the limitations of autograft, but is limited by the need for rigorous tissue screening, processing, and preservation methods to minimize the risk of immunogenicity or transmitting pathogens, and these procedures can compromise other aspects of graft function [1–3]. Therefore, a large number of synthetic bone graft substitutes have been investigated as alternatives and many are used clinically, including porous calcium phosphate ceramics and cements, collagenous sponges and putties, and various composites thereof [1–3,6].

The use of an absorbable collagen sponge to deliver osteoinductive recombinant human bone morphogenetic protein-2 (rhBMP-2) has comprised the most commercially successful synthetic bone graft substitute (InFuse®, Medtronic Somafor Danek) due to demonstrated potency in regenerating bone [6–8], although clinical efficacy has been clouded by controversy surrounding BMP dosing, complications, and off-label use [8,9]. Type I collagen is advantageous as a scaffold biomaterial due to partially mimicking the extracellular matrix (ECM) of bone for cell attachment, undergoing enzymatic degradation for cellular resorption, enabling cross-linking for tailored properties, and preparing highly porous scaffolds via freeze-drying [7,10–13]. However, collagen scaffolds

☆ *Funding sources:* U.S. Army Medical Research and Materiel Command (W81XWH-07-1-0662 and W81XWH-09-1-0741).

* Corresponding author at: Department of Aerospace and Mechanical Engineering, Bioengineering Graduate Program, 148 Multidisciplinary Research Building, University of Notre Dame, Notre Dame, IN 46556, USA. Tel.: +1 (574) 631 7003.
E-mail address: rroeder@nd.edu (R.K. Roeder).

http://dx.doi.org/10.1016/j.actbio.2015.01.031
1742-7061/

are limited by weak mechanical properties [12,13], such that clinical use is restricted to spatially confined and mechanically shielded sites, e.g., within an interbody spinal fusion cage.

Hydroxyapatite (HA) reinforced collagen scaffolds have been investigated as a means to improve mechanical properties and provide bioactivity, while further mimicking the ECM of bone [14–25]. HA–collagen scaffolds have been shown to support the attachment and proliferation of osteoblasts and osteoblast-like cells [15,21–24]. HA–collagen scaffolds were also recently shown to exhibit greater or comparable new bone formation *in vivo* when implanted alone compared to when implanted as a cell carrier or BMP delivery vehicle in ectopic and orthotopic models [26–28] for reasons that are not yet well understood. Thus, HA–collagen scaffolds have shown promise as a synthetic bone graft substitute and tissue engineering scaffold.

HA–collagen scaffolds are most commonly prepared by freeze drying a suspension of collagen fibrils and HA particles [14–19,22–28], or precipitating HA within a freeze-dried collagen scaffold [16,20,21]. Highly porous (>90%) freeze-dried scaffolds are readily fabricated, but exhibit a relatively small pore size, typically <100 μm. A pore size >300 μm is generally thought to be most advantageous for cellular infiltration, vascularization, and bone in growth [29]. Freeze-drying also results in a scaffold architecture with inherently thin struts, typically ~1–3 μm in thickness, which readily buckle and therefore limit compressive stiffness and strength even with HA reinforcement. Compressive moduli for freeze-dried HA–collagen scaffolds under hydrated conditions have been reported up to ~200–300 kPa in highly oriented scaffolds [18] or using HA whisker reinforcements [25], but are more commonly ~1–20 kPa [20–23,25,26]. Thus, the mechanical properties of HA–collagen scaffolds have remained less than ideal for surgical handling, fixation (e.g., with a pin), and bearing osteogenic loads during healing.

Therefore, the objectives of this study were to (1) prepare HA–collagen scaffolds with improved architecture and mechanical properties to overcome the limitations of freeze-dried scaffolds, (2) demonstrate cell infiltration and bioactivity *in vitro*, and (3) demonstrate angiogenesis and osteogenesis *in vivo*. HA–collagen scaffolds were prepared by concentrating a suspension of collagen fibrils, compression molding a mixture of HA, collagen, and paraffin microspheres, cross-linking the collagen matrix, and leaching the paraffin porogen. Effects of the scaffold porosity, HA reinforcement morphology, and HA volume fraction on the scaffold permeability, scaffold mechanical properties, and *in vitro* cellular behavior were investigated. Finally, *in vivo* angiogenesis and osteogenesis were investigated after subcutaneous ectopic implantation of HA–collagen scaffolds in mice.

2. Materials and methods

2.1. Raw materials

Soluble type I bovine collagen was received at a concentration of 3.2 mg/mL in 0.01 M HCl (DM-1, Devro Medical PLC, Glasgow, UK). The collagen solution was adjusted to physiological pH (7.4) and ionic strength (0.05 M) by adding the appropriate amounts of 1 M NaOH (Sigma–Aldrich, St. Louis, MO) and 10× Dulbecco's phosphate buffered saline (PBS, Sigma–Aldrich), respectively. Aliquots from the collagen solution (20 mL) were placed in an incubator overnight at 40 °C and the resulting collagen gels, still at a collagen concentration of ~3.2 mg/mL, were disrupted using a tissue homogenizer (Polytron PT1200, Kinematica, Lucerne, Switzerland) for 30 s. Collagen fibril suspensions were then centrifuged at 6000*g* for 30 min (Sorvall RC-6 Plus, Thermo Scientific, Waltham, MA) to concentrate the collagen fibrils to ~180 mg/mL and combined into a stock suspension which was stored at 8 °C until further use.

Single crystal HA whiskers were precipitated under hydrothermal conditions using the chelate decomposition method and conditions previously reported to result in a mean (± standard deviation) length and aspect ratio of 18 (8.9) μm and 7.9 (3.4), respectively [30,31]. An equiaxed HA powder was obtained commercially (Product #21221, Fluka Chemical Co., Buchs, Switzerland). The as-received powder was ground using a mortar and pestle to minimize agglomerates, and stored at 90 °C to remove residual moisture. The mean (± standard deviation) particle diameter of this powder was previously reported as 1.3 (0.4) μm [31], which was comparable to the width of the HA whiskers.

A paraffin microsphere porogen was produced using methods adapted from the literature [32]. Briefly, 40 g of a low melting point paraffin (Paraplast X-TRA®, Sigma–Aldrich) was heated to 90 °C, added to 400 mL of a solution containing 25 wt% sucrose (American Sugar Refining, West Palm Beach, FL) in deionized (DI) water at 80 °C, and rapidly stirred for 1 h to form a visually homogeneous emulsion. The emulsion was subsequently poured into 2 L of ice water to solidify the paraffin microspheres which were collected, washed five times with DI water to remove residual sucrose, and dried in a vacuum desiccator for 24 h at room temperature. Paraffin microspheres were fractionated to a size range of 300–425 μm using a shaker sieve (Ro-Tap® RX-29, W.S. Tyler, Mentor, OH) and stored in a sealed container at −20 °C. The sieved paraffin microspheres exhibited a mean diameter (± standard deviation) of 370 (56) μm as measured by optical microscopy by sampling over 250 microspheres collected from multiple batches.

2.2. Scaffold fabrication

HA reinforcements were added to the concentrated collagen fibril suspension in amounts calculated to result in 0, 20, 40, 60, and 80 vol% HA within collagen after removal of water, and stirred by hand for ~5 min until uniformly distributed. Paraffin microspheres were then folded into the HA–collagen suspension by hand using a spatula in amounts designed to produce scaffolds with 85% or 90% porosity by volume. The HA–collagen-paraffin suspension was loaded into a 6 mm diameter pellet die and compression molded at 1 MPa for 1 min. As-molded scaffolds were 3–5 mm in height depending on the amount of suspension added to the die and were subsequently dried at 37 °C for 24–48 h. Paraffin microspheres were leached by soaking scaffolds in successive solutions of 2× 100% hexane, 50/50 hexane/ethanol, and 4× 100% ethanol for at least 6 h each. The volume of each leaching solution was at least 20 times greater than the volume of the immersed scaffolds.

After compression molding and porogen leaching, the collagen matrix was crosslinked for 12 h under gentle agitation in a solution containing 20 mM *N*-(3-dimethylaminopropyl)-*N*′-ethylcarbodiimide hydrochloride (EDC, Sigma–Aldrich) and 8 mM *N*-hydroxysuccimide (NHS, Sigma–Aldrich) in 80/20 ethanol/DI water with pH adjusted to 7.4 by 0.1 M HCl. The concentration of EDC was adjusted such that the EDC:NHS:collagen binding site ratio was 5:2:1, which was previously shown to maximize collagen crosslinking [33]. Scaffolds were subsequently washed three times in 100% ethanol to remove unreacted EDC and stored in ethanol at 4 °C until further use.

2.3. Scaffold architecture and microstructure

The percent porosity (P) of as-prepared scaffolds fabricated with 85% or 90% target porosity and reinforced with 0, 20, 40, 60, or 80 vol% HA whiskers or powder (n = 3/group) was calculated as,

$$P = \left(1 - \frac{\rho_{scaffold}}{\rho_{material}}\right) \cdot 100 \quad (1)$$

where $\rho_{scaffold}$ is the apparent scaffold density and $\rho_{material}$ is the scaffold material density [22,23]. The apparent scaffold density was determined from the dry scaffold mass and volume measured using a digital mass balance (±0.0001 g) and digital electronic calipers (±0.01 mm), respectively. The scaffold material density was calculated from the volume fraction of HA within the scaffold material and the bulk densities of HA and collagen which were assumed to be 3.16 and 1.23 g/cm^3, respectively [25].

The architecture of representative scaffolds was imaged by micro-computed tomography (micro-CT, μCT-80, Scanco Medical AG, Brüttisellen, Switzerland) at 10 μm resolution, 70 kVp voltage, 114 μA current, and 400 ms integration time with slices oriented transverse to the vertical axis of the cylindrical scaffolds. The standard aluminum beam filter was removed for collagen scaffolds without HA reinforcement due to the low attenuation of these scaffolds. Grayscale images were smoothed by Gaussian filtration with sigma = 0.8 and support = 1. Three-dimensional reconstructions were created by segmenting grayscale images using a global threshold calibrated by the scaffold porosity determined from Eq. (1).

The microstructure of representative scaffolds was imaged by scanning electron microscopy (SEM) to examine pore interconnections and scaffold strut surfaces. Prior to leaching the paraffin porogen, scaffolds were transversely sectioned using a scalpel blade to expose the internal structure. After porogen leaching and crosslinking, scaffolds were dried at 40 °C for 24 h to remove residual moisture, mounted onto SEM stubs, and sputter coated with 10 nm iridium (208HR, Cressington Scientific Instruments Ltd., Watford, UK). Scaffolds were imaged (Evo 50, LEO Microscopy Ltd., Cambridge, UK) at an acceleration voltage of 10–15 kV and a working distance of 7–10 mm.

2.4. Mechanical properties

The mechanical properties of scaffolds fabricated with 85% or 90% target porosity and reinforced with 0, 20, 40, 60 and 80 vol% HA whiskers or powder (n = 5/group, except n = 3/group for 0 vol% HA) was measured in unconfined uniaxial compression. Scaffolds were rehydrated in PBS for 24 h at room temperature prior to testing. All scaffolds were approximately 6 mm in diameter and 3–5 mm in height. Note that minor variability in the scaffold height did not influence the measured compressive modulus (p = 0.55, MANCOVA). Scaffolds were loaded in unconfined uniaxial compression at a displacement rate of 0.05 mm/s to ~50% strain using an electromagnetic test instrument (ElectroForce 3300, Bose Corp., Eden Prairie, MN). Load and displacement data were collected at 10 Hz using a 5 lb load cell (MBP-5, Interface, Scottsdale, AZ) and linear variable displacement transducer (LVDT), respectively. Apparent stress and strain were calculated based upon the dimensions of the rehydrated scaffolds measured prior to loading using digital calipers (±0.01 mm). The zero strain point was set at first region of the stress–strain curve exhibiting a slope of 5 kPa or higher within a 2% strain range. The scaffold compressive modulus was measured as the maximum slope of the stress–strain curve over a 5% strain range within 0–20% strain (Fig. 1). The slope was determined by linear least squares regression and the correlation coefficient (R^2) was greater than 0.95 for each scaffold. This approach was used instead of a fixed strain range because the elastic collapse stress and strain increased with increasing HA reinforcement [25]. Finally, the elastic recovery and durability of representative scaffolds was characterized by loading in cyclic uniaxial compression at 1 Hz to 50% strain for up to 100,000 cycles.

2.5. Scaffold permeability

The fluid permeability of scaffolds fabricated with 85% or 90% target porosity and reinforced with 60 and 80 vol% HA whiskers or powder (n = 3/group) was measured using a forced flow apparatus [23,34]. Scaffolds reinforced with ⩽40 vol% HA were too compliant for reliable measurements using the forced flow apparatus. Scaffolds were rehydrated by soaking in 100% ethanol for 6 h, followed by PBS for 24 h. Scaffolds, typically 5.75–5.85 mm in diameter, were mounted within a 5.65 mm inner diameter tube leading to a pressure head. Scaffold permeability (m^2) was calculated using Darcy's law as,

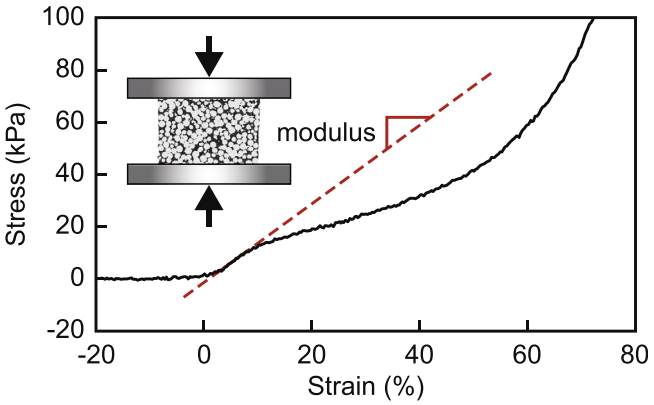

Fig. 1. Stress–strain curve for a HA–collagen scaffold showing the compressive modulus measured as the maximum slope (dashed line) fit by linear least squares regression over a 5% strain range within 0–20% strain [25].

$$K = \frac{Q \cdot \mu \cdot h}{A \Delta P} \tag{2}$$

where Q is the measured flow rate (m^3/s), μ is the fluid viscosity (Pa s), h is the height of the scaffold (m), A is the scaffold cross-sectional-area (m^2), and ΔP is the pressure drop (Pa) across the scaffold. The pressure exerted by the pressure head was calculated as $P = \rho \cdot g \cdot H$, where ρ is the density of the fluid, g is the gravitational acceleration, and H is the height of the pressure head. The required time for the flow of 5–10 mL of PBS was measured using a digital stopwatch and typically ranged 10–240 min depending on the scaffold permeability.

2.6. In vitro cell activity and infiltration

In vitro bioactivity was investigated by seeding murine adipose-derived stromal cells (mASCs) on scaffolds with 85% porosity and 0, 40, or 80 vol% HA whisker reinforcements (n = 11/group). mASCs were extracted from freshly harvested mouse adipose tissue using methods described in detail elsewhere [35] and expanded through two passages in growth media consisting of Dulbecco's modified Eagle's medium (DMEM, Mediatech, Manassas, VA) supplemented with 10% fetal bovine serum (FBS, Omega, Trazana, CA), and 1% penicillin/streptomycin (Mediatech) at 5% CO_2 and 37 °C. Scaffolds, 6 mm in diameter and 3 mm height, were sterilized by soaking in 100% ethanol for 24 h and rehydrated in sterile PBS overnight. Scaffold pore spaces were partially drained using sterile absorbent paper and placed into tissue culture plate wells previously coated with ~500 μL of a 1% agarose solution to prevent cell attachment. Cells were seeded from 75 μL aliquots of media containing $1.12 \cdot 10^6$ cells/mL placed onto the top surface of scaffolds for an initial seeding density of 10^6 cells/cm^3 of scaffold. After 1 h incubation at 5% CO_2 and 37 °C, each well was filled with 1.5 mL osteogenic differentiation media consisting of growth media (DMEM, 10% FBS, 1% pen/strep) supplemented with 100 μg/mL ascorbic acid (Sigma–Aldrich), 10 mM beta-glycerophosphate (Sigma–Aldrich), and 50 ng/mL rhBMP-6 (R&D Systems, Minneapolis,

MN). Scaffolds were cultured for 1, 7 and 14 d with media replaced every 2–3 days.

Total DNA and alkaline phosphatase (ALP) activity was measured for scaffolds at each time point ($n = 3$/group/time point). Scaffolds were removed from wells and rinsed in sterile PBS for ~1 min to remove excess media. Cells were lysed by placing the scaffold into 1 mL of 1% Triton X-100 (Sigma–Aldrich) in DI water and scaffolds were manually pulverized using a sterile polytetrafluoroethylene pestle. The mixture was rapidly vortexed for ~30 s and the lysate separated from the scaffold debris by centrifuging at 1000*g* for 1 min. The lysate was extracted and stored in individual Eppendorf tubes at −80 °C until further use. The total DNA content in the scaffold lysate was measured using a commercially available fluorescent DNA assay kit (Quant-iT PicoGreen, Invitrogen, Carlsbad, CA) and microplate reader (Victor3, Perkin Elmer, Waltham, MA). Alkaline phosphatase (ALP) activity was measured using a colorimetric assay kit (SensoLyte pNPP, Anaspec, San Jose, CA) and reported normalized to the total DNA (ALP/DNA).

One additional scaffold per group was cultured for 1 and 14 d for electron microscopy. Scaffolds were removed from wells, rinsed for ~10 min in sterile PBS, and fixed in 1 vol% glutaraldehyde in PBS for 90 min at 4 °C. Fixed scaffolds were rinsed in PBS for several hours, dehydrated by soaking in sequential solutions containing 5%, 10%, 25%, 50%, 75%, 90%, 95% and 100% ethanol in PBS, and dried at room temperature for 24 h. Transverse sections were prepared with a scalpel to expose the scaffold interior, mounted on SEM stubs, and sputter coated with 2 nm iridium (208HR, Cressington Scientific Instruments). Specimens were imaged in an SEM (Evo 50, LEO Microscopy Ltd.) using an accelerating voltage of 5–10 kV and a working distance of 7–10 mm.

In vitro cell infiltration was investigated by seeding passage 7 human adipose-derived stromal cells (hASCs, Zen-Bio Inc., Research Triangle Park, NC) on scaffolds with 85% porosity and 0 or 40 vol% HA whisker reinforcements ($n = 3$/group). Scaffolds, 3 mm in diameter and height, were prepared from rehydrated scaffolds using a biopsy punch, sterilized by soaking in 100% ethanol for 24 h, and rehydrated in sterile PBS overnight. Scaffold pore spaces were partially drained using sterile absorbent paper and placed into tissue culture plate wells previously coated with ~500 μL of a 1% agarose solution to prevent cell attachment. Cells were seeded from 30 μL aliquots of media placed onto the top surface of scaffolds for an initial seeding density of $4{\cdot}10^6$ cells/cm^3 of scaffold. After 1 h incubation at 5% CO_2 and 37 °C, each well was filled with 1.5 mL osteogenic media (DMEM, 10% FBS, 1% pen/strep, 100 μg/mL ascorbic acid, 10 mM beta-glycerophosphate) and cells were cultured 14 d with media replaced every 2–3 days. Scaffolds were removed from wells, rinsed for ~10 min in sterile PBS, fixed overnight in 4% paraformaldehyde, embedded in freezing medium (Tissue-Tek® O.C.T.™, Sakura Finetek, Torrance, CA), and cryosectioned at 6 μm. Sections were mounted on glass slides, stained by hematoxylin and eosin (H&E, VWR, Radnor, PA) and imaged using transmitted light microscopy (Eclipse ME600, Nikon Instruments, Melville, NY).

2.7. In vivo angiogenesis and osteogenesis

In vivo angiogenesis and osteogenesis were investigated by implanting scaffolds ($n = 3$) with 85% porosity and 40 vol% HA whisker reinforcements in ectopic subcutaneous pockets in the dorsal cervical region of 4 week old, female athymic nude mice (Harlan Laboratories, Indianapolis, IN) for 8 weeks [36]. All protocols were approved by the University of Notre Dame Institutional Animal Care and Use Committee (IACUC). Scaffolds, 3 mm in diameter and height, were prepared from rehydrated scaffolds using a biopsy punch, sterilized by soaking in 100% ethanol for 24 h, and rehydrated in sterile PBS overnight. Mice were anesthetized by intraperitoneal delivery of a cocktail containing 100 mg/mL ketamine (Butler-Schein, Dublin, OH), 20 mg/mL xylazine (Butler-Schein) and 10 mg/mL acepromazine (Butler-Schein) in sterile saline at a volumetric dose of $10{\cdot}W$–50 μL, where W is the mouse body weight (g). Scaffolds were implanted in each mouse through a small incision in the center of the dorsal region. The incision was closed with one autoclip which was removed approximately 10 d post-implantation after the wound was healed. Mice were sacrificed and scaffolds were excised at 8 weeks post-implantation.

All scaffolds were imaged by micro-CT (Bioscan NanoCT, Mediso Medical Imaging Systems, Budapest Hungary) at 10 μm resolution, 70 kVp voltage, 100 μA current, and 600 ms integration time for 720 projections. Scaffolds were imaged immediately before implantation and explants were imaged after overnight fixation in 4% paraformaldehyde. Micro-CT images were median filtered to reduce noise. The bone volume (BV) was measured by segmenting images at a threshold of 1900, which corresponded to ~294 mg HA/cm^3 using a custom calibration phantom [37]. *De novo* bone formation was measured by the percent difference in thresholded BV between the implant and explant.

For histology, explants were subsequently rinsed with PBS, decalcified in 0.5 M ethylenediaminetetraacetic acid (EDTA), cryopreserved in a series of sucrose solutions in PBS, equilibrated in optimal cutting temperature (OCT) compound (Tissue-Tek® O.C.T.™, Sakura Finetek) for 3 h, frozen in dry ice-cooled isopentane, and stored at −80 °C. Embedded explants were cryosectioned at 7–9 μm and transferred to gelatin subbed slides, which were dried at 37 °C for 2 h and then stored at −80 °C. Slides were warmed and dried prior to all staining procedures. Sections were warmed to room temperature and stained by H&E (VWR).

Immunolabeling was performed to label new blood vessels positive for CD31 and new osteoid positive for osteocalcin (OCN). For CD31, antigen retrieval was performed at 90 °C for 5 min in 1 mM EDTA with 0.05% Tween-20 (Sigma–Aldrich) at pH 8.0. Sections were cooled to room temperature, rinsed with PBS, and blocked with 1% donkey serum (Jackson ImmunoResearch, West Grove, PA), 0.3 M glycine (Fisher Scientific, Pittsburgh, PA) in PBS for 30 min at room temperature. Primary CD31 antibody (R&D Systems, Minneapolis, MN) was subsequently applied at 10 μg/mL in blocking solution overnight at 4 °C. After rinsing slides with PBS, the secondary antibody (AlexaFluor568 donkey anti-goat, Life Technologies, Carlsbad, CA) was diluted to 1:200 by volume in 1% bovine serum albumin (BSA, EMD Millipore, Billerica, MA) in PBS and applied for 1 h at room temperature. Finally, sections were counterstained with 4′,6-diamidino-2-phenylindole (DAPI, Vector Laboratories, Burlington, CA), rinsed with PBS, and mounted in an aqueous medium. For OCN, sections were hydrated in PBS, subjected to heat-mediated antigen retrieval as described above, and blocked in 1% normal goat serum (Jackson ImmunoResearch), 0.3 M glycine for 30 min at room temperature. Primary antibody (OCN rabbit polyclonal, Abcam, Cambridge, MA) was diluted to 1:1000 by volume and applied in 1% BSA in PBS overnight at 4 °C. Sections were rinsed with PBS, incubated with the fluorescent secondary antibody (goat anti-rabbit, Life Technologies) diluted to 1:200 by volume in 1% BSA in PBS for 1 h at room temperature, counterstained with DAPI, and mounted in an aqueous medium.

2.8. Statistical analysis

Differences between the measured and target scaffold porosity were investigated using a Student's *t*-test with a hypothesized mean set to the target porosity (JMP 8.1, SAS Inc., Cary, NC). Multiple analysis of variance (MANOVA) was used to investigate the effects of the HA reinforcement volume fraction, HA morphology,

and porosity level, on the scaffold porosity, permeability and compressive modulus. Two-way ANOVA was used to investigate the effects of the HA reinforcement volume fraction and days in culture on ALP activity (ALP/DNA). A log transform was used for permeability and ALP/DNA data to provide a normal distribution for statistical analysis. *Post-hoc* comparisons were performed using Tukey's HSD test. The level of significance for all tests was set at $p < 0.05$.

3. Results and discussion

3.1. Scaffold architecture and microstructure

Scaffolds were prepared with 85–90% porosity and 0–80 vol% HA whisker or powder reinforcements, and exhibited a hierarchical structure (Fig. 2) with characteristics designed to be favorable for osteointegration. Scaffold porosity was uniformly distributed, spherical, and interconnected with a mean size of ~300–400 μm (Fig. 2), which reflected the size and morphology of the leached paraffin microspheres. Importantly, scaffold pores >300 μm in size are known to be favorable for osteointegration [29]. Scaffold struts ranged ~3–100 μm in thickness due to being formed in the space between paraffin microspheres (Fig. 2). Therefore, the pore size and strut thickness were significantly greater than that exhibited by freeze-dried HA–collagen scaffolds [20–25]. HA reinforcements were able to be uniformly mixed in the collagen matrix as evidenced by uniform X-ray attenuation in micro-CT image slices. HA whiskers or powder were thus embedded in the collagen matrix to act as mechanical reinforcements and were also exposed on strut surfaces to act as bioactive sites for protein adsorption and cell attachment (Fig. 2c). HA reinforcements, and HA whiskers in particular, also provided a microscale surface roughness (Fig. 2c), which is known to enhance cell attachment [38].

The pooled mean (± standard deviation) measured porosity of scaffolds was 85.7 (3.9) and 89.2 (2.7)%, respectively, for a target porosity of 85% and 90%. Thus, differences between the measured and designed target porosity were not significantly different ($p > 0.21$ *t*-test) and the difference in the measured porosity between each target porosity level was statistically significant ($p < 0.0001$, ANOVA). These results indicated that scaffolds were able to be prepared at a target porosity with reasonable reliability. The measured porosity was also decreased for scaffolds with increased HA reinforcement levels ($p < 0.05$, ANOVA) and for HA whiskers versus powder ($p < 0.0001$, ANOVA), possibly due to increased rigidity of the HA–collagen mixture during molding, but these effects occurred within the variability at each target porosity level and were therefore small and of less importance.

The collagen matrix density is often overlooked, but critical for preparing mechanically robust scaffolds. HA–collagen scaffolds in this study were prepared from a suspension of collagen fibrils concentrated to ~180 mg/cm^3. A higher collagen fibril density was only previously achieved in dense, highly-aligned collagen fibril bundles [39]. Previous studies which recognized the importance of the collagen matrix density on scaffold mechanical properties achieved a maximum collagen fibril density of ~140 mg/cm^3 [40,41]. Therefore, the scaffold architecture (strut thickness), HA reinforcement, and collagen matrix density were all expected to result in HA–collagen scaffolds with significantly improved mechanical properties.

3.2. Mechanical properties

The mechanical properties of scaffolds prepared with 85% or 90% porosity and reinforced with 0, 20, 40, 60 and 80 vol% HA whiskers or powder were measured in unconfined uniaxial compression. All scaffolds exhibited stress–strain curves characteristic of highly porous, elastic foams (Fig. 1). The compressive modulus was increased with increased HA reinforcement ($p < 0.0001$), decreased porosity ($p < 0.0001$), and for HA whiskers vs. powder ($p < 0.0005$, MANOVA), as expected (Fig. 3). HA reinforcement enabled up to an order of magnitude increase in compressive modulus compared with unreinforced collagen scaffolds prepared by the same methods (Fig. 3). The HA–collagen scaffolds in this study exhibited a compressive modulus that ranged ~60–1000 kPa, compared with ~5–300 kPa for freeze-dried HA–collagen scaffolds [17–23,25] and 1–20 kPa for absorbable collagen sponges used clinically [12,13]. Thus, the compressive modulus was at least one order of magnitude greater than comparable freeze-dried HA–collagen scaffolds and two orders of magnitude greater than absorbable collagen sponges used clinically. Scaffolds reinforced with 80 vol% HA became brittle, but scaffolds reinforced with up to 60 vol% HA were highly elastic, completely recovering from cyclic deformations of up to 50% compressive strain for at least 100,000 cycles (Fig. 4, Supplementary Data in Appendix B). These results suggest that the HA–collagen scaffolds in this study exhibited mechanical properties which are well-suited for surgical handling, fixation, and partially bearing osteogenic loads during bone regeneration.

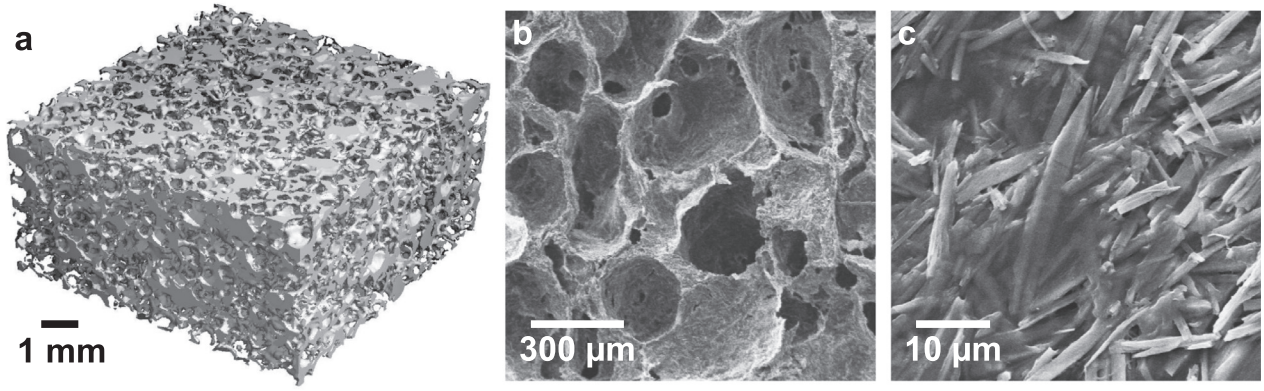

Fig. 2. The hierarchical structure of HA–collagen scaffolds prepared with 90% porosity and 80 vol% HA whiskers: (a) segmented micro-CT reconstruction showing the three-dimensional architecture for a 4 × 4 × 2 mm scaffold section, (b) SEM micrograph of the internal microstructure showing spherical, interconnected pores created by the paraffin porogen and densified struts composed of HA reinforcements embedded within a high density (~180 mg/mL) cross-linked collagen matrix, and (c) higher magnification SEM micrograph of the scaffold surface showing HA whiskers exposed on strut surfaces.

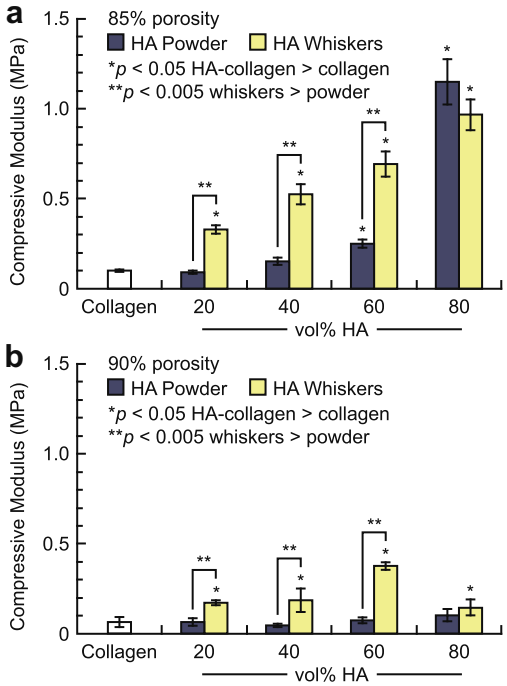

Fig. 3. Compressive modulus of HA–collagen scaffolds with (a) 85% or (b) 90% porosity and 0, 20, 40, 60, and 80 vol% HA whiskers or powder. Error bars show one standard deviation of the mean. HA reinforcement resulted in up to an order of magnitude increase in the compressive modulus compared with collagen scaffolds (*$p < 0.05$, HA–collagen > collagen, Tukey's HSD). HA whiskers provided a greater reinforcing effect compared with HA powder at 20, 40, and 60 vol% HA (**$p < 0.005$, HA whiskers > powder, Tukey's HSD). Scaffolds with 85% porosity exhibited a significantly increased compressive modulus compared with scaffolds with 90% porosity ($p < 0.0001$, MANOVA), such that a decrease in porosity of only 5% resulted in an increase in compressive modulus of ~40–1000%.

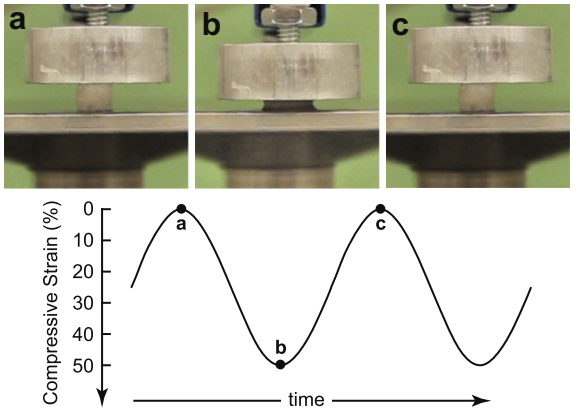

Fig. 4. Video frames and a schematic loading waveform showing the fully recoverable elastic deformation exhibited by HA–collagen scaffolds with 85% porosity and up to 60 vol% HA (40 vol% shown) during cyclic compression to 50% strain. The video is available as Supplementary Data in Appendix B.

The effect of HA reinforcement was more pronounced in scaffolds reinforced with HA whiskers compared with HA powder (Fig. 3). HA whiskers provided a greater reinforcing effect compared with HA powder at 20, 40, and 60 vol% HA ($p < 0.005$, HA whiskers > powder, Tukey's HSD), which are the levels of HA reinforcement most likely to be used in implants, but not at 80 vol% HA. HA whiskers were effective in reinforcing collagen scaffolds under all conditions, but HA powder was ineffective in reinforcing collagen scaffolds with 85% porosity at 20 and 40 vol% HA and 90% porosity at all levels of HA. These results suggest that HA whiskers can be used to enhance the mechanical properties of HA–collagen scaffolds. Moreover, HA–collagen scaffolds with 90% porosity and reinforced with 20–60 vol% HA whiskers were able to exceed the compressive modulus of scaffolds with 85% porosity at equal levels of HA powder reinforcement (Fig. 3). This result suggests that HA whiskers can be used to compensate for the loss of mechanical properties in higher porosity scaffolds.

HA whiskers have been demonstrated to provide improved tensile, compressive and fatigue properties compared with HA powder reinforcements in a variety of polymers due to enhanced stress transfer from the matrix polymer to elongated reinforcements and whisker alignment [25,31,42–44]. Moreover, elongated and oriented HA reinforcements were previously shown to be a critical factor enabling the mechanical properties achieved by native bone tissue [45]. However, despite the significant improvements described above, the compressive modulus of the HA–collagen scaffolds in this study was still substantially lower than the compressive modulus of 100-1000 MPa exhibited by human trabecular bone at a similar level of porosity [46]. Differences in compressive modulus between scaffolds reinforced with HA whiskers and powder may have also been influenced by the lower measured porosity of scaffolds reinforced with HA whiskers ($p < 0.0001$, ANOVA), but these differences were small in magnitude (<3%) and therefore unlikely to account for a significant portion of the large observed differences in compressive modulus.

The effect of HA reinforcement was also more pronounced in scaffolds with 85% porosity compared with 90% porosity (Fig. 3). The compressive modulus of scaffolds with 85% and 90% porosity was increased from ~100 to ~1000 kPa, and ~60 to ~400 kPa with HA whisker reinforcement, respectively. Thus, the compressive modulus of scaffolds with a comparable level of porosity (90%) to freeze-dried HA–collagen scaffolds was ~200% greater than freeze-dried HA–collagen scaffolds, likely due to a greater thickness of scaffold struts (~3–100 μm) which were more readily reinforced by HA. The uniformly thin struts in freeze-dried collagen scaffolds, typically ~1–3 μm in thickness, limits the incorporation of HA reinforcements [25]. The compressive modulus of scaffolds with a 85% porosity was at least one order of magnitude greater than freeze-dried HA–collagen scaffolds [17–23,25]. Thus, the differences in compressive modulus between scaffolds with 85% and 90% porosity demonstrated that a decrease in porosity of only 5% resulted in a disproportionate increase in compressive modulus of ~40–1000% at a given level of HA reinforcement (Fig. 3). This result suggested that a small decrease in porosity could be highly beneficial for mechanical function if scaffold permeability is not compromised.

3.3. Scaffold permeability

The fluid permeability of scaffolds prepared with 85% or 90% porosity and reinforced with 60 and 80 vol% HA whiskers or powder was measured by forced flow using Darcy's law. The pooled mean (± standard deviation) scaffold permeability was $7.9 \cdot 10^{-13}$ ($3.6 \cdot 10^{-13}$) m^2 and the overall range of permeability measurements spanned $4 \cdot 10^{-13}$ to $19 \cdot 10^{-13}$ m^2. The measured permeability was not significantly influenced by scaffold porosity, HA reinforcement content, or HA morphology ($p > 0.12$, MANOVA).

The permeability of a scaffold is a key functional property governed by the total porosity, pore size, and pore interconnectivity, and is thus indicative of the likelihood of cells infiltrating a scaffold [29,34,47–49]. The similarity in scaffold permeability measured across experimental groups suggests that permeability was primarily governed by smaller pore interconnections, typically observed to be 50–100 μm in size (Fig. 2b), formed by contact between paraffin porogen microspheres prior to leaching. This

further suggests that the size and number of these pore interconnections was similar across HA–collagen scaffolds with 85% or 90% porosity and reinforced with 60 and 80 vol% HA whiskers or powder, which was qualitatively observed in SEM (Fig. 2b).

HA–collagen scaffolds in this study exhibited similar permeability to freeze-dried HA–collagen scaffolds, which were previously reported to exhibit permeability up to $45{\cdot}10^{-13}$ m^2 [23]. The same freeze-dried HA–collagen scaffolds supported the attachment and proliferation of pre-osteoblasts *in vitro* and bone regeneration *in vivo* [23], although cellular infiltration was not directly characterized. Therefore, scaffolds in the present study were also expected to support cell infiltration, as reported below. Moreover, the lack of significant differences in permeability between scaffolds with 85% and 90% porosity justified the use of scaffolds with 85% porosity in subsequent *in vitro* and *in vivo* experiments investigating cell infiltration and angiogenesis, as reported below.

3.4. In vitro cell activity and infiltration

Alkaline phosphatase (ALP) activity was measured *in vitro* over 14 d in osteogenic media after seeding murine adipose-derived stromal cells (mASCs) on scaffolds prepared with 85% porosity and reinforced with 0, 40, and 80 vol% HA whiskers. The effects of HA content ($p < 0.0001$) and days in culture ($p < 0.0001$) on ALP activity (ALP/DNA), as well as their interaction ($p < 0.05$, ANOVA), were statistically significant. ALP/DNA was increased at days 7 and 14 compared with day 1 for each level of HA content ($^{*}p < 0.0005$, vs. day 1, Tukey's HSD), and was greater for HA–collagen scaffolds compared with collagen alone at days 7 and 14 ($^{**}p < 0.01$, Tukey's HSD) (Fig. 5a). In contrast, the total DNA content was increased with time ($p < 0.001$) and for collagen alone compared with HA–collagen scaffolds ($p < 0.05$, ANOVA). For both ALP activity and total DNA, differences between scaffolds with 40 and 80 vol% HA were not statistically significant. Therefore, over 14 d in osteogenic media mASCs exhibited greater proliferation on collagen scaffolds and greater differentiation on HA–collagen scaffolds, which was consistent with the known bioactivity of HA in collagen scaffolds [15,23,24,26] and alone [50]. Moreover, due to the known behavior of the same cell line in the same media [51], the results suggest that the HA–collagen scaffolds were osteogenic. Finally, after 14 d mASCs were observed to be adhered to scaffold strut surfaces (Fig. 5b) and bridging internal pore spaces (Fig. 5c) for both collagen and HA–collagen scaffolds. Scaffold strut surfaces were covered in deposited extracellular matrix or osteoid.

Cell infiltration was measured *in vitro* over 14 d in osteogenic media after seeding human adipose-derived stromal cells (hASCs) on scaffolds prepared with 85% porosity and reinforced with 0 and 40 vol% HA whiskers. H&E stained histological sections revealed that hASCs were able to completely infiltrate 3 mm diameter scaffolds after 14 d in culture (Fig. 6). Collagen scaffolds exhibited contraction and peripheral pore collapse during culture (Fig. 6a). In contrast, HA–collagen scaffolds were able to retain their original size, shape, and pore architecture (Fig. 6b). This result suggests that resistance to cell-mediated contraction was enabled by the greater compressive modulus of collagen scaffolds reinforced with 40 vol% HA whiskers (~500 kPa) compared with collagen alone (~100 kPa) (Fig. 3a). Scaffold contraction can close pores and reduce permeability, inhibiting nutrient and waste transport to/from cells in the center of scaffolds [52,53].

HA–collagen scaffolds exhibited bioactivity while collagen scaffolds did not, consistent with other studies [15,23,24,26], but there was no difference in ALP activity between collagen scaffolds reinforced with 40 and 80 vol% HA (Fig. 5). Therefore, *in vitro* cell infiltration and *in vivo* osteogenesis were only investigated in collagen scaffolds reinforced with 40 vol% HA whiskers. However, the minimum level of HA reinforcement (<40 vol%) to achieve suitable bioactivity was not determined in this study and should be investigated further. Furthermore, while HA reinforcement levels greater than 40 vol% exhibited no additional effect on *in vitro* bioactivity, the effect of the greater stiffness of scaffolds with greater than 40 vol% HA on *in vitro* and *in vivo* performance should also be investigated further.

3.5. In vivo angiogenesis and osteogenesis

In vivo angiogenesis and osteogenesis were investigated after ectopic implantation of acellular scaffolds with 85% porosity and 40 vol% HA whisker reinforcements in mice (Fig. 7a). After 8 weeks of implantation, capillaries were visually evident on the explant (Fig. 7b) and *de novo* bone formation was evidenced by a mean (± standard deviation) difference in thresholded bone volume (ΔBV) of 61 (7)% measured by micro-CT for explants. Micro-CT measurements were inclusive of the HA–collagen scaffold material

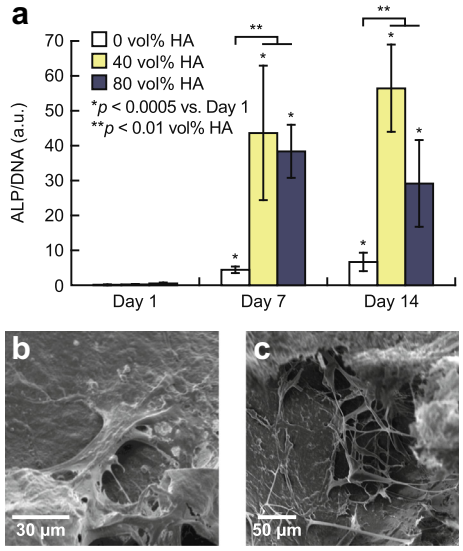

Fig. 5. (a) The ALP activity of mASCs cultured in HA–collagen scaffolds with 85% porosity and 0, 40, and 80 vol% HA whiskers at days 1, 7, and 14. Error bars show one standard deviation of the mean. ALP activity (ALP/DNA) was increased at days 7 and 14 compared with day 1 for each level of HA content ($^{*}p < 0.0005$, vs. day 1, Tukey's HSD), and was greater for HA–collagen scaffolds compared with collagen alone at days 7 and 14 ($^{**}p < 0.01$, Tukey's HSD). Representative SEM micrographs showing (b) mASCs adhered to scaffold strut surfaces (0 vol% HA) and (c) bridging internal pore spaces (80 vol% HA).

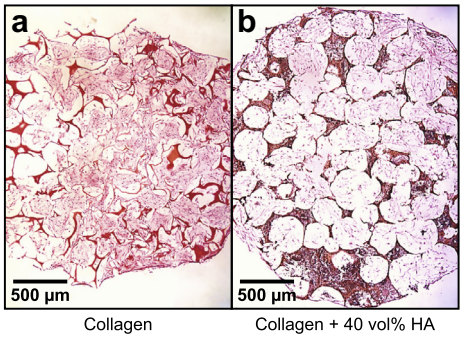

Fig. 6. Histologic sections (H&E stained) showing the infiltration of hASCs throughout HA–collagen scaffolds with 85% porosity and (a) 0 vol% and (b) 40 vol% HA whiskers after 14 d in culture. Collagen scaffolds exhibited contraction and peripheral pore collapse during culture. In contrast, HA–collagen scaffolds were able to retain their original size, shape, and pore architecture.

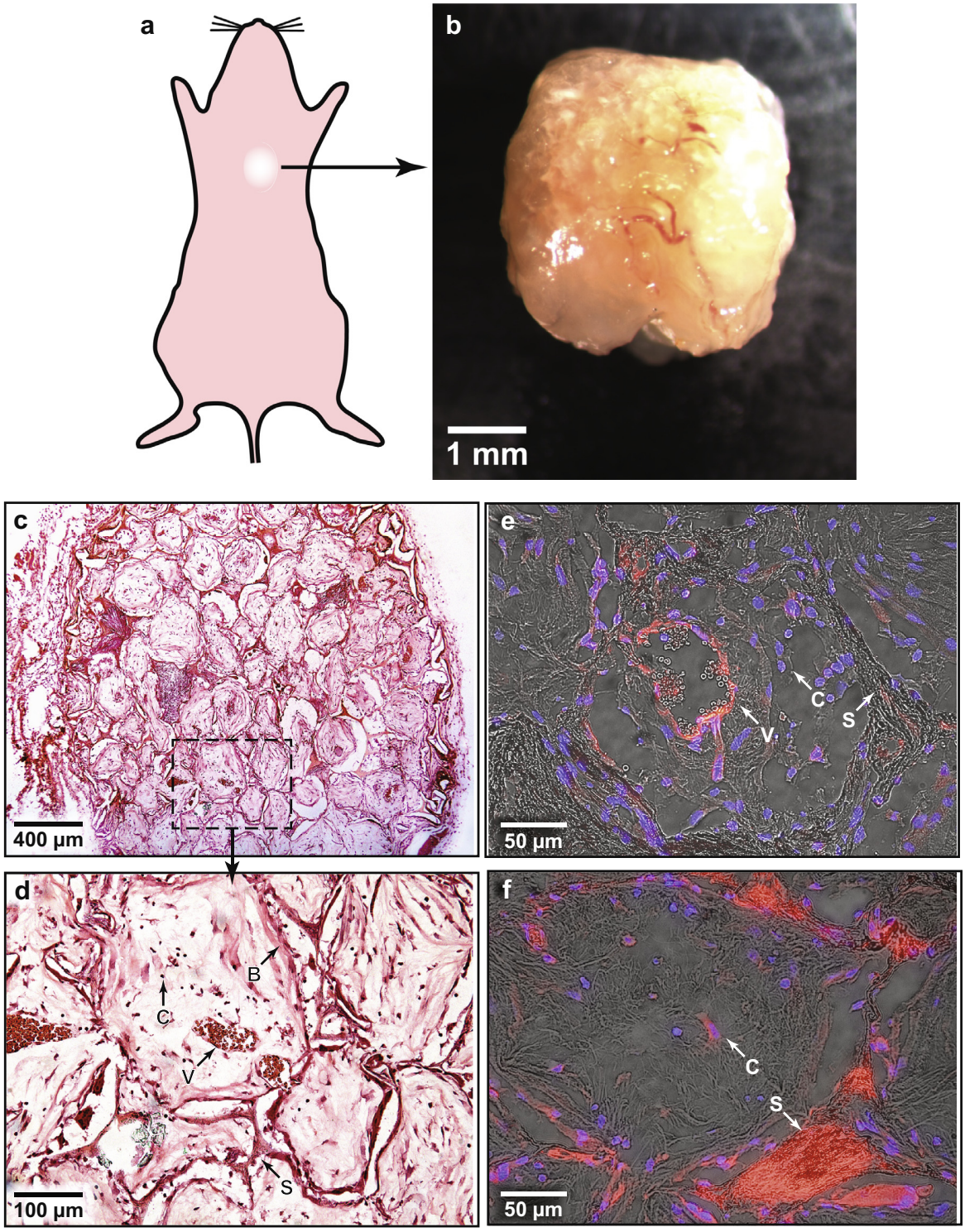

Fig. 7. HA–collagen scaffolds with 85% porosity and 40 vol% HA whiskers were (a) implanted in the ectopic subcutaneous pockets of 4 week old, female athymic nude mice for 8 weeks. (b) Photograph of a representative explants showing visually apparent capillaries evident of significant vascularization. Histologic sections (H&E stained) of explanted scaffolds showing (c) the entire scaffold cross-section and (d) a higher magnifications image showing widespread vascularization (V), cellular invasion (C), and immature bone (B) or osteoid adjacent to the scaffold (S). Immunolabeled histologic sections showing infiltrating mouse cells (blue, DAPI) and positive staining (red) for (e) CD31 and (f) osteocalcin (OCN) confirmed the presence of neovascularization and immature bone, respectively. Co-localization of DAPI and OCN indicates the expression of OCN by infiltrating mouse cells.

and new bone formation, but were reasonably assumed to reflect new bone formation since the HA reinforcements would not be expected to undergo significant resorption in 8 weeks.

H&E stained histologic sections revealed the presence of widespread vascularization, cellular invasion, and immature bone or osteoid adjacent to the scaffold after 8 weeks implantation (Fig. 7c and d). The presence of vasculature and immature bone was confirmed by positive immunohistochemical staining for CD31 (Fig. 7e) and OCN (Fig. 7f), respectively. Co-localization of DAPI and OCN indicated the expression of OCN by infiltrating

mouse cells. Thus, acellular HA–collagen scaffolds were demonstrated to induce angiogenesis and osteogenesis after ectopic implantation by recruiting endogenous cell populations, suggesting that the scaffolds were osteoinductive.

Freeze-dried HA–collagen scaffolds were previously shown to induce osteogenesis after intramuscular ectopic implantation in rat hindlimbs in the absence of exogenous cell and growth factor delivery [28]. Subcutaneous ectopic implantation was chosen in the present study due to surgical simplicity and exhibiting a lower inductive potential compared with intramuscular pouch models [54,55]. The low number of endogenous bone-forming cells in the intradermal environment makes subcutaneous ectopic models advantageous for investigating osteoinduction. Thus, HA–collagen scaffolds were osteoinductive due to providing a favorable microenvironment for the adsorption of endogenous growth factors [56], the infiltration of endogenous cell populations (Figs. 6 and 7c,d), and the differentiation of endogenous cells (Fig. 5 and 7e,f). A number of previous investigations have reported various calcium phosphate biomaterials to be osteoinductive after subcutaneous ectopic implantation [56–58]. However, calcium phosphate ceramics are often limited clinically by brittle mechanical properties. In contrast, the HA–collagen scaffolds in this study exhibited a combination of suitable compressive stiffness (Fig. 3), fully recoverable elastic deformation (Fig. 4), and osteoinduction (Fig. 7).

4. Conclusions

HA–collagen scaffolds were prepared using new methods which resulted in high porosity (85–90%), interconnected pores ~300–400 μm in size, struts of greater thickness (~3–100 μm) than freeze-dried scaffolds, and a matrix with a relatively high collagen fibril density (~180 mg/cm^3) containing 0–80 vol% HA whisker or powder reinforcements. The scaffold architecture, permeability, and composition were shown to be conducive to the infiltration and differentiation of ASCs *in vitro*, as well as angiogenesis and osteogenesis *in vivo* after subcutaneous ectopic implantation, suggesting that the scaffolds are osteoinductive. HA–collagen scaffolds exhibited a compressive modulus of up to ~1 MPa, which was at least one order of magnitude greater than comparable freeze-dried HA–collagen scaffolds and two orders of magnitude greater than absorbable collagen sponges used clinically. Moreover, scaffolds reinforced with up to 60 vol% HA exhibited fully recoverable elastic deformation upon cyclic loading to 50% compressive strain for up to 100,000 cycles, suggesting that the scaffolds are able to withstand surgical handling, fixation, and partially bearing osteogenic loads during bone regeneration. Therefore, the HA–collagen scaffolds in this study appear to be suitable for clinical use as a synthetic bone graft substitute and tissue engineering scaffold and offer improvements over existing freeze-dried HA–collagen scaffolds and absorbable collagen sponges used clinically.

Acknowledgments

This research was supported by the U.S. Army Medical Research and Materiel Command (W81XWH-07-1-0662 and W81XWH-09-1-0741). The authors acknowledge the Freimann Life Science Center at the University of Notre Dame for the care of animals and the Notre Dame Integrated Imaging Facility for SEM and *in vivo* computed tomography.

Appendix A. Figures with essential color discrimination

Certain figures in this article, particularly Figs. 1 and 3–7, are difficult to interpret in black and white. The full color images can be found in the on-line version, at http://dx.doi.org/10.1016/j.actbio.2015.01.031.

Appendix B. Supplementary data

Supplementary data associated with this article can be found, in the online version, at http://dx.doi.org/10.1016/j.actbio.2015.01.031.

References

[1] Greenwald AS, Boden SD, Goldberg VM, Khan Y, Laurencin CT, Rosier RN. Bone-graft substitutes: facts, fictions and applications. J Bone Joint Surg Am 2001;83A:98–103.
[2] Giannoudis PV, Dinopoulos H, Tsiridis E. Bone substitutes: an update. Injury 2005;36:S20–7.
[3] Friedlaender GE, Mankin HJ, Goldberg VM, editors. Bone Grafts and Bone Graft Substitutes. Rosemont, IL: American Academy of Orthopaedic Surgeons; 2006.
[4] Arrington E, Smith W, Chambers H, Bucknell A, Davino N. Complications of iliac crest bone graft harvesting. Clin Orthop Rel Res 1996;329:300–9.
[5] Myeroff C, Archdeacon M. Autologous bone graft: donor site and techniques. J Bone Joint Surg Am 2011;93A:2227–36.
[6] De Long Jr WG, Einhorn TA, Koval K, McKee M, Smith W, Sanders R, Watson T. Bone grafts and bone graft substitutes in orthopaedic trauma surgery. J Bone Joint Surg 2007;89A:649–58.
[7] Geiger M, Li RH, Friess W. Collagen sponges for bone regeneration with rhBMP-2. Adv Drug Delivery Rev 2003;55:1613–29.
[8] Grabowski G, Cornett CA. Bone graft and bone graft substitutes in spine surgery: current concepts and controversies. J Am Acad Orthop Surg 2013;21:51–60.
[9] Carragee EJ, Hurwitz EL, Weiner BK. A critical review of recombinant human bone morphogenetic protein-2 trials in spinal surgery: emerging safety concerns and lessons learned. Spine J 2011;11:471–91.
[10] Khor E. Methods for the treatment of collagenous tissues for bioprostheses. Biomaterials 1997;18:95–105.
[11] O'Brien FJ, Harley BA, Yannas IV, Gibson LJ. The effect of pore size on cell adhesion in collagen-GAG scaffolds. Biomaterials 2005;26:433–41.
[12] Harley BA, Leung JH, Silva EC, Gibson LJ. Mechanical characterization of collagen–glycosaminoglycan scaffolds. Acta Biomater 2007;2007(3):463–74.
[13] Tierney CM, Haugh MG, Liedl J, Mulcahy F, Hayes B, O'Brien FJ. The effects of collagen concentration and crosslink density on the biological, structural and mechanical properties of collagen-GAG scaffolds for bone tissue engineering. J Mech Behav Biomed Mater 2009;2:202–9.
[14] Wang RZ, Cui FZ, Lu HB, Wen HB, Ma CL, Li HD. Synthesis of nanophase hydroxyapatite/collagen composite. J Mater Sci Lett 1995;14:490–2.
[15] Liu L, Zhang L, Ren B, Wang F, Zhang Q. Preparation and characterization of collagen–hydroxyapatite composite used for bone tissue engineering scaffold. Artif Cells Blood Substit Biotechnol 2003;31:435–48.
[16] Wahl DA, Czernuska JT. Collagen–hydroxyapatite composites for hard tissue repair. Eur Cells Mater 2006;11:43–56.
[17] Wahl DA, Sachlos E, Liu C, Czernuszka JT. Controlling the processing of collagen–hydroxyapatite scaffolds for bone tissue engineering. J Mater Sci – Mater Med 2007;18:201–9.
[18] Yunoki S, Ikoma T, Tsuchiya A, Monkawa A, Ohta K, Sotome S, et al. Fabrication and mechanical and tissue ingrowth properties of unidirectionally porous hydroxyapatite/collagen composite. J Biomed Mater Res 2007;80B:166–73.
[19] Gelinsky M, Welzel PB, Simon P, Bernhardt A, König U. Porous three-dimensional scaffolds made of mineralised collagen: preparation and properties of a biomimetic nanocomposite material for tissue engineering of bone. Chem Eng J 2008;137:84–96.
[20] Al-Munajjed AA, O'Brien FJ. Influence of a novel calcium–phosphate coating on the mechanical properties of highly porous collagen scaffolds for bone repair. J Mech Behav Biomed Mater 2009;2:138–46.
[21] Al-Munajjed AA, Plunkett NA, Gleeson JP, Weber T, Jungreuthmayer C, Levingstone T, et al. Development of a biomimetic collagen–hydroxyapatite scaffold for bone tissue engineering using a SBF immersion technique. J Biomed Mater Res 2009;90B:584–91.
[22] Cunniffe GM, Dickson GR, Partap S, Stanton KT, O'Brien FJ. Development and characterisation of a collagen nano-hydroxyapatite composite scaffold for bone tissue engineering. J Mater Sci – Mater Med 2010;21:2293–8.
[23] Gleeson JP, Plunkett NA, O'Brien FJ. Addition of hydroxyapatite improves stiffness, interconnectivity and osteogenic potential of a highly porous collagen-based scaffold for bone tissue engineering. Eur Cells Mater 2010;20:218–30.
[24] Jones GL, Walton R, Czernuszka J, Griffiths SL, Haj El AJ, Cartmell SH. Primary human osteoblast culture on 3D porous collagen–hydroxyapatite scaffolds. J Biomed Mater Res 2010;94A:1244–50.
[25] Kane RJ, Roeder RK. Effects of hydroxyapatite reinforcement on the architecture and mechanical properties of freeze-dried collagen scaffolds. J Mech Behav Biomed Mater 2012;7:41–9.
[26] Lyons FG, Al-Munajjed AA, Kieran SM, Toner ME, Murphy CM, Duffy GP, et al. The healing of bony defects by cell-free collagen-based scaffolds compared to

stem cell-seeded tissue engineered constructs. Biomaterials 2010;31:9232–43.
[27] Lyons FG, Gleeson JP, Partap S, Coghlan K, O'Brien FJ. Novel microhydroxyapatite particles in a collagen scaffold: a bioactive bone void filler? Clin Orthop Rel Res 2014:1318–28.
[28] Murphy CM, Schindeler A, Gleeson JP, Yu N, Cantril LC, Mikulec K, et al. A collagen–hydroxyapatite scaffold allows for binding and co-delivery of recombinant bone morphogenetic proteins and bisphosphonates. Acta Biomater 2014;10:2250–8.
[29] Karageorgiou V, Kaplan D. Porosity of 3D biomaterial scaffolds and osteogenesis. Biomaterials 2005;26:5474–91.
[30] Roeder RK, Converse GL, Leng H, Yue W. Kinetic effects on hydroxyapatite whiskers synthesized by the chelate decomposition method. J Am Ceram Soc 2006;89:2096–104.
[31] Roeder RK, Sproul MS, Turner CH. Hydroxyapatite whiskers provide improved mechanical properties in reinforced polymer composites. J Biomed Mater Res 2003;67A:801–12.
[32] Ma PX, Choi J-W. Biodegradable polymer scaffolds with well-defined interconnected spherical pore network. Tissue Eng 2001;7:23–33.
[33] Olde Damink LHH, Dijkstra PJ, van Luyn MJA, van Wachem PB, Nieuwehuis P, Feijen J. Cross-linking of dermal sheep collagen using a water-soluble carbodiimide. Biomaterials 1996;17:765–73.
[34] O'Brien FJ, Harley BA, Waller MA, Yannas IV, Gibson LJ, Prendergast PJ. The effect of pore size on permeability and cell attachment in collagen scaffolds for tissue engineering. Technol Health Care 2007;15:3–17.
[35] Malladi P, Xu Y, Chiou M, Giaccia AJ, Longaker MT. Effect of reduced oxygen tension on chondrogenesis and osteogenesis in adipose-derived mesenchymal cells. Am J Physiol Cell Physiol 2006;290:C1139–46.
[36] Weiss HE, Roberts SJ, Schrooten J, Luyten FP. A semi-autonomous model of endochondral ossification for development tissue engineering. Tissue Eng A 2012;18:1334–43.
[37] Deuerling JM, Rudy DJ, Niebur GL, Roeder RK. Improved accuracy of cortical bone mineralization measured by polychromatic micro-computed tomography using a novel high mineral density composite calibration phantom. Med Phys 2010;37:5138–45.
[38] Deligianni DD, Katsala ND, Koutsoukos PG, Missirlis YF. Effect of surface roughness of hydroxyapatite on human bone marrow cell adhesion, proliferation, differentiation and detachment strength. Biomaterials 2001;22:87–96.
[39] Saeidi N, Karmelek KP, Paten JA, Zareian R, DiMasi E, Ruberti JW. Molecular crowding of collagen: a pathway to produce highly-organized collagenous structures. Biomaterials 2012;33:7366–74.
[40] Yunoki S, Ikoma T, Tanaka J. Development of collagen condensation method to improve mechanical strength of tissue engineering scaffolds. Mater Char 2010;61:907–11.
[41] Yunoki S, Sugiura H, Ikoma T, Kondo E, Yasuda K, Tanaka J. Effects of increased collagen-matrix density on the mechanical properties and *in vivo* absorbability of hydroxyapatite–collagen composites as artificial bone materials. Biomed Mater 2011;6:015012.
[42] Converse GL, Yue W, Roeder RK. Processing and tensile properties of hydroxyapatite-whisker-reinforced polyetheretherketone. Biomaterials 2007;28:927–35.
[43] Kane RJ, Converse GL, Roeder RK. Effects of the reinforcement morphology on the fatigue properties of hydroxyapatite reinforced polymers. J Mech Behav Biomed Mater 2008;1:261–8.
[44] Roeder RK, Converse GL, Kane RJ, Yue W. Hydroxyapatite reinforced polymer biocomposites for synthetic bone substitutes. JOM 2008;60:38–45.
[45] Deuerling JM, Yue W, Espinoza Orías AA, Roeder RK. Specimen-specific multiscale model for the anisotropic elastic constants of human cortical bone. J Biomechanics 2009;42:2061–7.
[46] Morgan EF, Bayraktar HH, Keaveny TM. Trabecular bone modulus-density relationships depend on anatomic site. J Biomechanics 2003;36:897–904.
[47] Murphy CM, Haugh MG, O'Brien FJ. The effect of mean pore size on cell attachment, proliferation and migration in collagen-glycosaminoglycan scaffolds for bone tissue engineering. Biomaterials 2010;31:461–6.
[48] Mitsak AG, Kemppainen JM, Harris MT, Hollister SJ. Effect of polycaprolactone scaffold permeability on bone regeneration in vivo. Tissue Eng A 2011;17:1831–9.
[49] Karande TS, Ong JL, Agrawal CM. Diffusion in musculoskeletal tissue engineering scaffolds: design issues related to porosity, permeability, architecture, and nutrient mixing. Ann Biomed Eng 2004;32:1728–43.
[50] Shu R, McMullen R, Baumann MJ, McCabe LR. Hydroxyapatite accelerates differentiation and suppresses growth of MC3T3-E1 osteoblasts. J Biomed Mater Res 2003;67A:1196–204.
[51] Kemmis CM, Vahdati A, Weiss HE, Wagner DR. Bone morphogenetic protein 6 drives both osteogenesis and chondrogenesis in murine adipose-derived mesenchymal cells depending on culture conditions. Biochem Biophys Res Comm 2010;401:20–5.
[52] Lee CR, Grodzinsky AJ, Spector M. The effects of cross-linking of collagen-glycosaminoglycan scaffolds on compressive stiffness, chondrocyte-mediated contraction, proliferation and biosynthesis. Biomaterials 2001;22:3145–54.
[53] Keogh MB, O'Brien FJ, Daly JS. Substrate stiffness and contractile behaviour modulate the functional maturation of osteoblasts on a collagen-GAG scaffold. Acta Biomater 2010;6:4305–13.
[54] Scott MA, Levi B, Askarinam A, Nguyen A, Rackohn T, Ting K, et al. Brief review of models of ectopic bone formation. Stem Cells Dev 2012;21:655–67.
[55] Habibovic P, Sees TM, van den Doel MA, van Blitterwijk CA, de Groot K. Osteoinduction by biomaterials—physicochemical and structural influences. J Biomed Mater Res 2006;77A:747–62.
[56] LeGeros RZ. Properties of osteoconductive biomaterials: calcium phosphates. Clin Orthop Rel Res 2002:81–98.
[57] Gosain AK, Song L, Riordan P, Amarante MT, Nagy PG, Wilson CR, et al. A 1-year study of osteoinduction in hydroxyapatite-derived biomaterials in an adult sheep model: Part I. Plast Reconstr Surg 2002;109:619–30.
[58] Yuan H, van Blitterwijk CA, de Groot K, de Bruijn JD. Cross-species comparison of ectopic bone formation in biphasic calcium phosphate (BCP) and hydroxyapatite (HA) scaffolds. Tissue Eng 2006;12:1607–15.